# A kinetic study of 2-propanol dehydration on carbon acid catalysts

J. Bedia, R. Ruiz-Rosas, J. Rodríguez-Mirasol *, T. Cordero

Chemical Engineering Department, School of Industrial Engineering, University of Málaga, Campus de Teatinos s/n, 29071 Málaga, Spain

## ARTICLE INFO

## ABSTRACT

Activated carbons with high surface acidity were obtained in a single step by chemical activation of hemp residues with $H_3PO_4$ and used as catalysts for the dehydration reaction of 2-propanol. Despite the washing process performed after the activation, the resulting carbons show a considerable amount of surface phosphorus as revealed by XPS. The surface acidity, predominantly of Brönsted type, was dependent on the amount of phosphorus retained on the carbon surfaces. Conversion of 2-propanol yielded only dehydration products, mostly propylene with a very low amount of di-isopropyl ether. The effect of a thermal treatment performed to carbon catalyst on the surface chemistry, acidity and dehydration activity was analyzed. A kinetic study of the catalytic dehydration of 2-propanol on the best carbon catalyst was carried out, where two different Langmuir–Hinshelwood mechanisms, via surface elimination reactions, E1 and E2, were analyzed. The rate expressions derived from both models fitted properly the experimental results and activation energy values of about 98 kJ/mol were obtained. The results indicate that the 2-propanol dehydration reaction takes place by an E2 elimination mechanism with strong E1 character.

© 2010 Elsevier Inc. All rights reserved.

## 1. Introduction

Flash pyrolysis of biomass produces liquid oil (bio-oil) constituted mostly by oxygenated compounds which, after the proper treatments, are of great interest as fuel [1,2]. Like the biomass precursor, this bio-oil contains almost negligible amount of nitrogen, sulfur and metals. However, transformation of bio-oil is necessary to reach a quality similar to that of the conventional fuel. Studies have been conducted to improve the quality of bio-oil as fuel through catalytic processes with inorganic acid solids [3–5]. Gayubo et al. [4] studied the catalytic transformation of several model components of biomass pyrolysis oil, such us phenols and alcohols (1 and 2-propanol, 1 and 2-butanol, . . .), over HZSM-5 zeolite obtaining mainly light olefins and aromatics.

Alcohol decomposition is also used as test reaction for the evaluation of the acid and base properties of catalysts. Alcohol dehydrogenation products (aldehydes and ketones) are preferentially formed on basic catalysts, while dehydration products (olefins and ethers) are favored when acidic sites are present [6]. It is generally accepted that 2-propanol decomposition over basic sites proceeds through an elimination reaction yielding acetone. Over acid sites, 2-propanol dehydrates to propylene and to di-isopropyl ether [7]. Propylene is a key building block for the petrochemical industry used for the production of polypropylene, acrylonitrile, propylene oxide, cumene, oxo-alcohols and other intermediates. Propylene demand has grown from 16.4 million tons in 1980 to 69.0 million tons in 2006, and the demand is expected to increase faster than supply up to 350 million tons in 2020 [8]. Nowadays, propylene is obtained from non-renewable sources mainly as by-product of ethylene production in stream crackers and from refinery in FCC streams. Therefore, the finding and developing of new processes for propylene production from renewable sources is of great interest from economical and environmental point of views.

Activated carbons are mainly used as adsorbent and catalyst supports. However, the special characteristics of these materials related to their porous structure and surface chemistry make them suitable to be used also as catalysts per se [9]. Activated carbons show some important advantages to be used as catalysts [10], like a high specific surface area, high thermal and chemical stability and the possibility to be obtained from many diverse materials including different types of lignocellulosic waste [11–14]. Carbon materials can be used as catalysts for acid/base reactions due to the presence of surface oxygen groups of acidic and/or basic character [15,16]. To increase the surface acidity, carbons are usually oxidized with different chemical compounds in order to introduce oxygen surface complexes [16,17]. The increase in the surface acidity is associated to the formation of carboxylic and lactonic groups, which show a low to moderate stability [18]. Chemical activation with phosphoric acid results in carbons with high thermal stability surface groups that provide high surface acidity. These groups decompose at temperatures higher than 700 °C producing CO and $CO_2$, as a consequence of the decomposition of oxygen–phosphorus surface groups formed during the activation process [19].

In this study, acid carbons were studied as catalysts for the selective catalytic dehydration of 2-propanol (as model compound

---

## Nomenclature

| | |
|---|---|
| $A_{BET}^{N_2}$ | apparent surface area ($m^2\,g^{-1}$) |
| $A_{DR}^{CO_2}$ | narrow micropore surface area ($m^2\,g^{-1}$) |
| $A_t^{N_2}$ | external surface area ($m^2\,g^{-1}$) |
| Da | Damköhler number |
| CARB | cationic species (carbocation or isopropoxide) |
| $d_p$ | particle diameter (cm) |
| $Ea_{CARB}$ | activation energy of the cationic species formation reaction ($kJ\,mol^{-1}$) |
| $Ea_{PROPY}$ | activation energy of the propylene formation reaction ($kJ\,mol^{-1}$) |
| $\Delta H_{ad}^0$ | standard enthalpy of adsorption ($kJ\,mol^{-1}$) |
| $\Delta H_{IPA}$ | enthalpy of adsorption of 2-propanol ($kJ\,mol^{-1}$) |
| $\Delta H_{PROPY}$ | enthalpy of adsorption of propylene ($kJ\,mol^{-1}$) |
| IPA | 2-propanol |
| $k_{CARB}$ | cationic species formation rate constant ($mol\,g^{-1}\,s^{-1}$) |
| $K_{IPA}$ | 2-propanol adsorption constant ($atm^{-1}$) |
| $k_{oCARB}$ | preexponential factor of the cationic species formation ($mol\,g^{-1}\,s^{-1}$) |
| $K_{oIPA}$ | preexponential factor of the 2-propanol adsorption ($atm^{-1}$) |
| $K_{oPROPY}$ | preexponential factor of the propylene adsorption ($atm^{-1}$) |
| $k_{oPROPY}$ | preexponential factor of the propylene formation ($mol\,g^{-1}\,s^{-1}$) |
| $k_{PROPY}$ | propylene formation rate constant ($mol\,g^{-1}\,s^{-1}$) |
| $K_{PROPY}$ | propylene adsorption constant ($atm^{-1}$) |
| $L_b$ | bed length (cm) |
| $n$ | reaction order |
| $m$ | molecular weight ($g\,mol^{-1}$) |
| $Pe_p$ | particle Peclet number |
| $P_{IPA}^o$ | 2-propanol partial pressure at the reactor inlet (atm) |
| $P_{IPA}$ | 2-propanol partial pressure (atm) |
| $P_{PROPY}$ | propylene partial pressure (atm) |
| PROPY | propylene |
| $R$ | universal gas constant ($R = 8.31\,J\,mol^{-1}\,K^{-1}$) |
| $Re_p$ | particle Reynolds number |
| $r_{CARB}$ | rate of cationic species formation ($mol\,s^{-1}\,g^{-1}$) |
| $r_{PROPY}$ | rate of propylene formation ($mol\,s^{-1}\,g^{-1}$) |
| $r_{IPA}$ | 2-propanol conversion rate ($mol\,s^{-1}\,g^{-1}$) |
| $\Delta S_{ad}^0$ | standard entropy of adsorption ($J\,mol^{-1}\,K^{-1}$) |
| $S_g^0$ | standard entropy in gas phase ($J\,mol^{-1}\,K^{-1}$) |
| Sdii | di-isopropyl ether selectivity |
| Sp | propylene selectivity |
| $T$ | temperature (K) |
| $V_{DR}^{CO_2}$ | narrow micropore volume ($cm^3\,g^{-1}$) |
| $V_{mes}^{N_2}$ | mesopore volume ($cm^3\,g^{-1}$) |
| $V_t^{N_2}$ | micropore volume ($cm^3\,g^{-1}$) |
| $W/F_{IPA}^o$ | 2-propanol space time ($g\,s\,mol^{-1}$) |
| $X$ | conversion |
| $X_{exp}$ | experimental conversion |
| $X_{IPA}$ | 2-propanol conversion |
| $X_{sim}$ | simulated conversion |

*Greek letters*

| | |
|---|---|
| $\varphi$ | Thiele modulus |
| $\eta$ | interphase internal effectiveness factor |
| $\eta_{ext}$ | interphase external effectiveness factor |
| $\theta_i$ | fractional coverage of species i |
| $\theta_V$ | fractional vacant acid sites |

of bio-oil) to propylene. Acid-activated carbons were obtained by chemical activation with $H_3PO_4$ of hemp residues in a single step, without the need for incorporating acid surface groups in a complementary stage by chemical oxidation of the carbon surface. The effect of the activation conditions and the surface oxygen groups on the catalytic dehydration of 2-propanol over the acid-activated carbons was investigated. A kinetic study of 2-propanol dehydration reaction on the carbon catalyst was carried out.

## 2. Experimental

### 2.1. Catalyst synthesis methods

Hemp stems supplied by Alsativa (Sociedad Cooperativa Agraria Andaluza del Cáñamo, Pórtugos, Granada) were used as precursor of the activated carbons. The preparation of the activated carbons is reported elsewhere [19]. The precursor was impregnated with 85% (w/w) $H_3PO_4$ aqueous solution at room temperature and dried for 24 h at 60 °C in a vacuum dryer. The impregnated hemp stems were activated under continuous $N_2$ flow (150 $cm^3$ STP/min) in a conventional tubular furnace. The activation temperature was reached at a heating rate of 10 °C/min and maintained for 2 h. Different activation temperatures (350–550 °C) and impregnation ratios (1,2), defined as $H_3PO_4$/precursor weight ratio, were studied. The activated samples were cooled inside the furnace under $N_2$ flow, then washed with distilled water at 60 °C until neutral pH and negative phosphate analysis in the eluate [20] and dried at 110 °C. The activated carbons obtained are denoted by the letter C followed by a number corresponding to the impregnation ratio and by a second number representing the activation temperature in degree Celsius.

### 2.2. Catalyst characterization

The surface chemistry of the samples was analyzed by temperature-programmed desorption (TPD), X-ray photoelectron spectroscopy (XPS) and Fourier transform infrared (FTIR) spectroscopy. TPD profiles were obtained in a custom quartz tubular reactor placed inside an electrical furnace. The samples were heated from room temperature up to 900 °C at a heating rate of 10 °C/min in a helium flow (200 $cm^3$ STP/min). The amounts of CO and $CO_2$ desorbed from the samples were monitored with non-dispersive infrared (NDIR) gas analyzers (Siemens ULTRAMAT 22), and the $H_2$ concentration was measured by a mass spectrometer (Pfeiffer Vacuum, OmniStar model). X-ray photoelectron spectroscopy (XPS) analyses of the samples were obtained using a 5700C model Physical Electronics apparatus, with Mg Kα radiation (1253.6 eV). For the analysis of the XPS peaks, the C1s peak position was set at 284.5 eV and used as reference to locate the other peaks. The fitting of the XPS peaks was done by least squares using Gaussian–Lorentzian peak shapes. Fourier transform infrared (FTIR) spectra were obtained using a Bruker Optics Tensor 27 FTIR spectrometer by adding 256 scans in the 4000–400 $cm^{-1}$ spectral range at 4 $cm^{-1}$ resolution. Pressed KBr pellets at a sample/KBr ratio of around 1:250 were used.

The total acidity and acid strength distribution of the catalysts were determined by temperature-programmed desorption of ammonia. The $NH_3$–TPD was performed using 80 mg of catalysts saturated with pure $NH_3$ at 100 °C. After saturation, the $NH_3$ weakly adsorbed was desorbed in a He flow at the adsorption temperature, until no $NH_3$ was detected in the outlet gas. The TPD was performed by raising the temperature up to 500 °C at a heating rate of 10 °C/min. Outlet $NH_3$ concentrations were measured by gas

chromatography using a thermal conductivity detector. The type of surface acidity (Brönsted or Lewis) was studied by adsorption and desorption of pyridine (Py) and 2,6-dimetilpyridine (DMPy) carried out in a thermogravimetric system (CI Electronics) at 100 °C. The inlet partial pressure of the organic bases was 0.02 atm, and it was established saturating He with the corresponding organic base in a saturator at controlled temperature. After saturation of the carbon, desorption is carried out at the adsorption temperature in Helium flow. FTIR analysis of the carbons with adsorbed Py and DMPy were performed.

### 2.3. 2-Propanol dehydration

The decomposition of 2-propanol (IPA) was carried out at atmospheric pressure in a quartz fixed bed microreactor (4 mm i.d.) placed inside a vertical furnace with temperature control, using 65 mg of catalyst (100–300 μm particle size) dispersed in 1 g of SiC. Nitrogen was saturated with 2-propanol (Sigma–Aldrich, 99.5%, HPLC grade) vapor by contact in a saturator. To avoid the condensation of 2-propanol or any reaction product, all the lines from the saturator to the chromatograph were heated above 120 °C. The concentrations of the reactant and the products were measured by online gas chromatography (Perkin–Elmer Autosystem GC, 50 m HP-1 methyl silicone capillary column, flame ionization detector) and by mass spectrometry (Pfeiffer Vacuum, OmniStar model). Standard conditions for 2-propanol dehydration on the catalysts were a 2-propanol partial pressure of 0.022 atm and a space time of 0.043 g s/μmol. For the kinetic study, the inlet 2-propanol partial pressure varied from 0.012 to 0.081 atm and the space time from 0.012 to 0.170 g s/μmol.

The conversion was defined as the molar ratio of 2-propanol converted to the 2-propanol supplied to the reactor. The selectivity for each product was defined as the molar ratio of each product to 2-propanol converted.

## 3. Results and discussion

### 3.1. Preparation and characterization of the catalysts

The preparation and characterization of the activated carbons are reported elsewhere [19]. Four different activated carbons were prepared, namely, C1-450, C2-350, C2-450 and C2-550. The isotherms of the carbons are modified type I, characteristic of carbons with a well-developed microporous structure and a significant contribution of mesoporosity. The carbons obtained present BET surface areas ($A_{BET}$) between 700 and almost 1500 m$^2$/g and show a significant amount of surface phosphorus, as a consequence of the activation procedure [14,19], which increases with the activation temperature and decreases with the impregnation ratio.

Carbon C1-450, which shows the highest phosphorus surface concentration [19], was submitted to successive TPD. Fig. 1 shows the evolution with temperature of CO, $CO_2$ and $H_2$ during three successive TPDs. A table with the total amount of CO, $CO_2$ and $H_2$ evolved for each TPD has been included in the figure. The CO profile of the first TPD is mainly characterized by a considerable amount of CO desorbed at high temperatures ($T > 700$ °C). This behavior, reported in the literature [21], could be associated to the decomposition of phosphorus groups of high thermal stability formed during the activation process. The amount of carboxylic, lactonic and anhydride groups, which decompose as $CO_2$ during the thermal treatment, is much lower, as indicates the lower amount of $CO_2$ than that of CO desorbed. It is noticeable the presence of high stable groups that decompose as $CO_2$ at temperatures higher than 700 °C. The evolution of $CO_2$ and CO at high temperatures might be due to the decomposition of stable O=C—O—P and
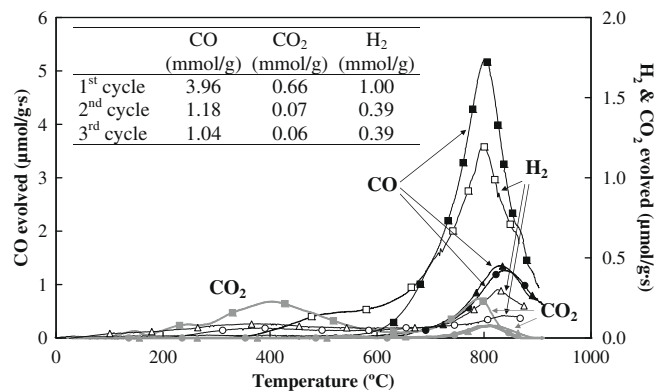


**Fig. 1.** CO (black closed symbols), $CO_2$ (gray closed symbols) and $H_2$ (open symbols) evolved with temperature during three consecutive TPDs (1st cycle: squares; 2nd cycle: triangles; 3rd cycle: circles) performed to C1-450 carbon.

C—O—P groups, respectively [19]. An alternative explanation for the $CO_2$ desorbed at high temperatures is that secondary reactions between the CO and the oxygen surface groups take place [19,22].

The second and third TPDs showed a little but constant presence of CO desorbed at high temperatures (850 °C) with a small peaks of $CO_2$ and $H_2$. The presence of C—O—$PO_3$ groups might explain these results. The oxygen bonded to C and P evolves as CO at high temperatures during the first TPD. The CO desorption generates active surface sites susceptible to be attacked probably by the P and the hydroxyl group linked to phosphorus, producing a C—$PO_2$—O—C type surface groups and $H_2$. This new group may produce, during the subsequent TPDs, a new desorption of CO at high temperature. The $CO_2$ evolution may be attributed to the secondary reactions previously commented. It is noteworthy the amount of gases evolved during the second and the third TPDs were similar suggesting a stabilization of the groups that desorbed at high temperatures. The high amount of desorbed $H_2$ may be a consequence of both the aromatic condensation and the dehydrogenation of the acid phosphates on the carbon surface.

Infrared spectroscopy (IR) provides information about the chemical structure of carbon catalysts. Fig. 2 shows the FTIR spectrum of the C1-450 carbon and of a sample obtained by carbonization of hemp cane at 450 °C denoted as C-450 [19]. The spectra of both carbons show bands at around 1570 cm$^{-1}$, characteristic of the aromatic ring stretching mode. The presence of these bands suggests the existence of single or multiple aromatic rings in the structure of the carbons. The presence of shoulders at 890, 820 and 760 cm$^{-1}$, due to C—H out-of-plane bend vibrations, supports the aromatic character of the carbons. The presence of aliphatic structures is suggested by the peaks at 2960, 2920 and
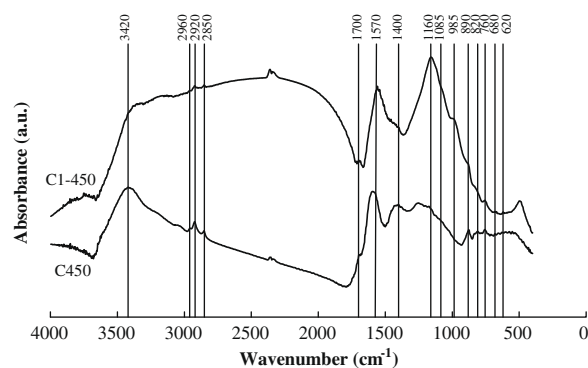


**Fig. 2.** FTIR spectrum of C1-450 carbon catalyst and C-450 carbon.

$2850\ cm^{-1}$ characteristic of aliphatic C—H stretching vibration, at $2960\ cm^{-1}$ due to methyl C—H asymmetric stretch and at $2920$ and $2850\ cm^{-1}$ as a consequence of methylene C—H asymmetric/symmetric stretch [23].

The presence of phenol groups is supported by the peak at $1400\ cm^{-1}$, characteristic of O—H bending vibrations [24]. The peak at around $1700\ cm^{-1}$ is characteristic of C=O absorption in carboxylic acids. The low intensity of these peaks indicates a lower amount of phenol and carboxylic groups compared with other oxygen groups of the carbon catalyst. The spectrum of C1-450 carbon displays a wide band between $1300$ and $900\ cm^{-1}$ with the maximum at $1160\ cm^{-1}$. A shoulder is observed at $1085\ cm^{-1}$. The adsorption in this region is generally found in oxidized carbons and is attributed to C—O stretching vibrations in acids, alcohols, phenol, ethers and esters [25,26].

It is interesting to point out that C1-450 carbon, with a significant P surface content [19], shows clearly a broad band between $1300$ and $900\ cm^{-1}$, almost not observed in the spectrum of C-450 carbon that contains a negligible amount of surface P [19]. This broad band between $1300$ and $900\ cm^{-1}$ is also assigned to several types of phosphorus groups formed during the chemical activation of carbons with phosphoric acid [23,27,28]. The strong intensity peak at $1160\ cm^{-1}$ is characteristic of the stretching vibrations of hydrogen-bonded P=O groups [29–31] from phosphates and polyphosphates of the O—C stretching vibrations in the P—O—C (aromatic) linkage [28,29] and of O=P—OH groups [28]. This supports the results previously discussed in the XPS analysis. The shoulder at $1085\ cm^{-1}$ is assigned to P—O$^-$ in acid phosphate esters and to the symmetrical vibration in polyphosphate chain P—O—P [32,33]. The presence of phosphate groups is supported by the peak at $620\ cm^{-1}$ and by the shoulder at $985\ cm^{-1}$, both characteristic of stretching vibrations of phosphate groups [28]. The shoulder at $985\ cm^{-1}$ is also associated to the P—O—C stretching vibration for pentavalent phosphorus [28]. The presence of C—P groups ($795$–$650\ cm^{-1}$) [31] is supported by the peaks located at $760$ and $680\ cm^{-1}$. The spectrum does not show bands' characteristic of P—H ($2500$–$2225\ cm^{-1}$) [31], which rule out the presence of phosphine derivates.

Fig. 3 shows the NH$_3$–TPD profiles for different carbon catalysts after adsorption and desorption of NH$_3$ at $100\ ^\circ C$. The desorption temperature indicates the acid strength of the sites, with weaker sites desorbing at lower temperatures. The C1-450 carbon shows the highest amount of NH$_3$ desorbed, confirming the higher acidity of this carbon. The total acidity, expressed as the total amount of NH$_3$ desorbed during the TPD, is reported in Fig. 3. The amount of desorbed NH$_3$ increases with the amount of surface phosphorus [19] revealed by XPS analyses, suggesting that the acidity of the carbons is related to the phosphorus retained on the carbon surface, probably associated to the OH groups in phosphates.
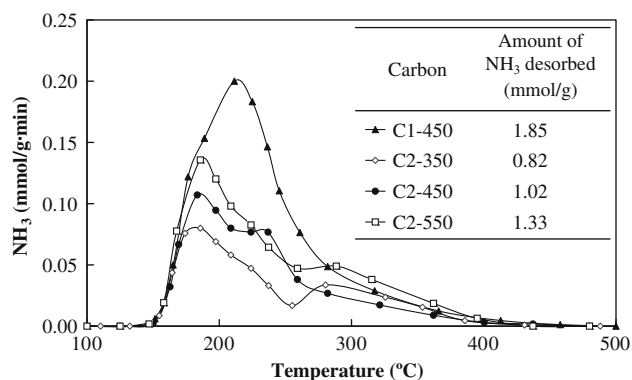
Chemisorption of basic molecules such as pyridine (Py) and 2,6-dimethylpyridine (DMPy) is often used to probe the acidity of solids [34–37]. Pyridine interacts with acidic sites because it has a lone electron pair at the nitrogen atom available for donation to a Lewis acidic site and because it can accept a proton from Brönsted sites. In contrast, 2,6-dimethylpyridine is selectively adsorbed on Brönsted acid sites because of its higher basicity and steric hindrance of the methyl groups [38,39]. The difference between the total amount of adsorbed pyridine and 2,6-dimethylpyridine corresponds to the amount of Lewis acid sites. Fig. 4 represents the adsorption and desorption kinetics of Py and DMPy on C1-450 carbon at $100\ ^\circ C$. The amounts of Py and DMPy retained after the desorption process (irreversible chemisorbed Py and DMPy) are very similar, suggesting that most of the acid sites of the carbon are Brönsted sites. Therefore, the chemical activation of biomasic residues with H$_3$PO$_4$ yields carbons with a predominantly Brönsted acidity. The amount chemisorbed of both organic bases is very similar to the amount of ammonia desorbed during the TPD (Fig. 3).

Fig. 5 represents the room temperature FTIR spectra of C1-450 activated carbon with adsorbed Py and DMPy. Interaction of pyridine, via the nitrogen lone-pair electrons, with aprotic (Lewis) and protonic (Brönsted) acid sites can be analyzed by following the ring vibration modes 8a and 19b, respectively [40]. The interaction of Py with Lewis type acid sites produces 8a vibration mode usually observed at around $1624\ cm^{-1}$ and 19b vibration mode at around $1452\ cm^{-1}$. The former was not observed, and the latter appeared in form of a low intensity shoulder suggesting a low presence of Lewis acid sites on the C1-450 carbon surface. The shoulder at $1574\ cm^{-1}$ is characteristic of weakly adsorbed (physisorbed) pyridine. The pyridine interaction with Brönsted acid sites is observed at $1587\ cm^{-1}$ for 8a vibration mode and at $1442\ cm^{-1}$ for 19b vibration mode. Both peaks are clearly observed in the Py-adsorbed spectra, supporting the results previously obtained in the TG analysis that the acid sites of the carbon surface are predominantly of Brönsted type. The band at $1483\ cm^{-1}$ could be associated to 19a vibration of pyridine ions. Further characterization of Brönsted acidity was performed by FTIR spectroscopy of adsorbed DMPy. This probe molecule is more sensitive to Brönsted acidity than it is pyridine. The FTIR spectrum of C1-450 carbon with DMPy adsorbed shows four adsorption bands at $1605$, $1589$, $1477$ and $1464\ cm^{-1}$. The last two bands can be assigned to weakly adsorbed (physisorbed) DMPy [35,41,42]. The bands at $1605$ and $1589\ cm^{-1}$ were attributed to DMPy molecules hydrogen-bonded to carbon surface [39,43,44], indicating the presence of Brönsted type acid sites on the carbon surface.

In order to analyze the role of the surface oxygenated groups in the acidity of the carbons and in the alcohol decomposition reaction, the C1-450 carbon was submitted to thermal treatments in



**Fig. 3.** NH$_3$–TPD profiles for the carbon catalysts.
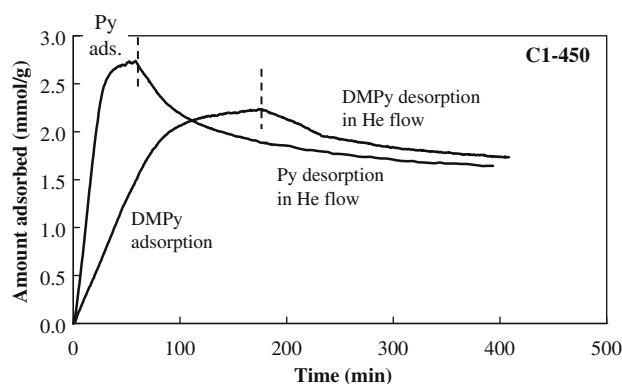


**Fig. 4.** Adsorption and desorption kinetics of pyridine (Py) and 2,6-dimethylpyridine (DMPy) on C1-450 carbon at $100\ ^\circ C$.
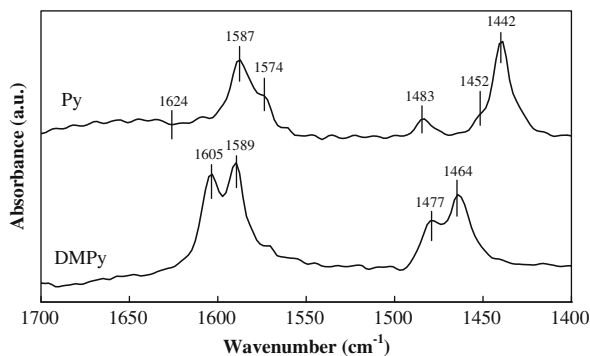
**Fig. 5.** FTIR spectra of C1-450 carbon catalyst after adsorption of pyridine (Py) and 2,6-dimethyl pyridine (DMPy).

**Table 1**
Mass surface concentration (%) determined by XPS quantitative analysis and total amount of $NH_3$ desorbed in the $NH_3$–TPD for C1-450-TT700 and C1-450-TT900.

|  | XPS C 1s | O 1s | P 2p | $NH_3$–TPD $NH_3$ desorbed (mmol/g) |
|---|---|---|---|---|
| C1-450-TT700 | 63.2 | 23.8 | 13.0 | n.m. |
| C1-450-TT900 | 66.4 | 19.1 | 14.0 | 1.23 |

n.m. = not measured.

inert atmosphere up to 700 and 900 °C. The carbons obtained are denoted as C1-450-TT700 and C1-450-TT900, respectively. Table 1 summarizes the mass surface concentration of C, O and P determined by XPS quantitative analysis of these carbons. The thermal treatment increases progressively the amount of surface phosphorus from 11%, for the original carbon [19], up to 14%, for the carbon treated at 900 °C. This might be due to the loss of oxygen surface groups during the thermal treatment that decreases the surface oxygen concentration and increases the carbon and phosphorus content at the external surface of the carbon. The thermal treatment also produces a significant decrease in the surface acidity, as reveals the lower amount of $NH_3$ desorbed for the C1-450-TT900 carbon (1.23 mmol/g) than that observed for the carbon C1-450 (1.85 mmol/g). Fig. 6 represents the P 2p zone of the carbons C1-450, C1-450-TT700 and C1-450-TT900. The phosphorus spectra were deconvoluted using two doublet peaks with an area ratio of 0.5 and a separation between peaks of 0.84 eV [45]. For the fitting, the position of the center of the peaks was allowed to vary ±0.2 eV, while the full width at half-maximum (FWHM) was varied between 0.80 and 1.5 eV. The P 2p zone is the result of the contribution of different phosphorus states. A main peak of doublet at a value around 134.2 eV can be assigned to the P groups
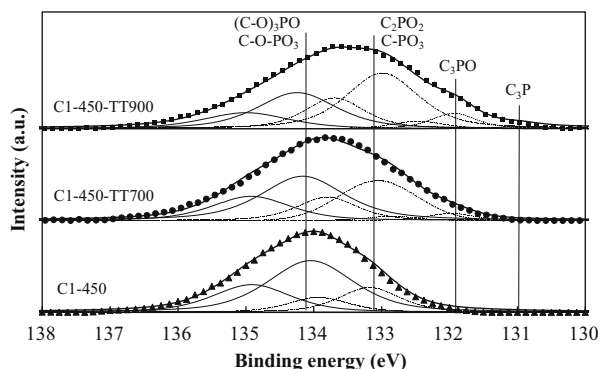


**Fig. 6.** XPS P 2p zone of carbons C1-450, C1-450-TT700 and C1-450-TT900.

bonded to a carbon site throughout an O atom ($C-O-PO_3$ and/or ($C-O)_3PO$)) [21], the binding energy of about 133.2 eV is characteristic of C—P bonding as in $C-PO_3$ and/or $C_2PO_2$ [21], and the value 132.0 eV of the main peak of the doublet is associated to $C_3PO$ groups [45]. Finally, a low intensity doublet peak with the main peak centered at around 131.0 eV is ascribed to $C_3P$ groups [45]. The thermal treatment results in a reduction in the binding energy of the maximum of the peaks and a displacement to lower binding energies of the entire signal, being this displacement greater at the highest thermal treatment temperature analyzed. This result suggests that the thermal treatment decreases the proportion of oxygen in the surface phosphorus groups, with a reduction in the most oxygenated phosphorus groups (($C-O-PO_3$ and/or ($C-O)_3PO$)) and an increase in the $C_3PO$ and $C_3P$ groups.

### 3.2. 2-Propanol catalytic dehydration

The catalytic decomposition of 2-propanol has been studied on different carbon catalysts in order to analyze the effect of phosphorus and oxygen surface groups. Also, a kinetic study has been carried out. To verify that axial dispersion problems are negligible, the following criterion is often used [46–48]:

$$\frac{L_b}{d_p} > \frac{20 \cdot n}{Pe_p} \cdot Ln\left(\frac{1}{1-X}\right) \qquad (1)$$

where $L_b$ is the bed length, $n$ is the reaction order, $X$ is the conversion, $d_p$ is the particle diameter and $Pe_p$ is the particle Peclet number. For large particle Reynolds number ($Re_p$) values, $Pe_p$ is about 2, whereas in the conditions used for laboratory reactors $Re_p$ is often low and therefore $Pe_p$ is lower than 2. For $Re_p < 1$, a value for $Pe_p$ of 0.5 has been suggested [49]. It has also been stated that criterion (1) is too conservative and that the factor 20 can be replaced by 8 [49]. In the conditions used in this study, the $Re_p$ number was 0.25 and so a value of 0.50 was chosen for the $Pe_p$ number. The value of $L_b/d_p$ was 100.0 and the values of the right-hand side of the Eq. (1) were 92.1 and 36.8 when using a factor of 20 and 8, respectively. Therefore, the effects of axial dispersion could be neglected.

The absence of external and internal mass transfer limitations was checked theoretically. The effect of the external mass transfer limitations was evaluated using the Damköler number, Da, i.e. the ratio of the chemical reaction rate to the mass transfer rate. An interphase external effectiveness factor, $\eta_{ext}$, was used to evaluate the influence of external mass transport on the global reaction rate. A value of 0.955 for $\eta_{ext}$ and a value of $4.66 \times 10^{-2}$ for Da number were obtained, respectively. These values confirmed the negligible external mass transfer effects. The absence of internal mass transfer limitation was evaluated using the isothermal intraphase internal effectiveness factor, $\eta$, which is a function of the Thiele modulus, $\varphi$. A value of 0.255 was obtained for the Thiele modulus and a value of 0.996 was obtained for the intraphase effectiveness factor. Therefore, internal mass diffusion effects were also negligible in the experimental conditions studied in this work.

The 2-propanol steady-state conversion as a function of the reaction temperature for different carbon catalysts is represented in Fig. 7. Conversion increases with the reaction temperature. There is no relation between the apparent surface area [19] and the 2-propanol steady-state conversions for the different carbon catalysts. The carbon C1-450, which shows the lowest surface area, displays the highest steady-state conversion, probably because of its higher acidity as measured with $NH_3$–TPD (Fig. 3 and Table 1). The increase in the activation temperature leads to carbons with higher conversions (C2-550 > C2-450 > C2-350). This suggests that the increase in the amount of phosphorus with the activation temperature produces carbons with higher surface acidity and resulting in higher 2-propanol steady-state conversions. On the
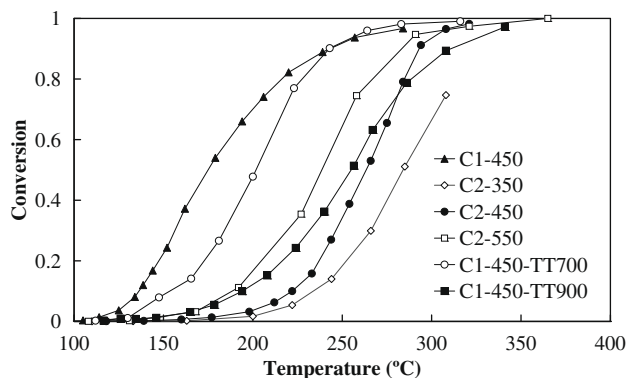
**Fig. 7.** Conversion of 2-propanol as a function of temperature for the C1-450 catalyst ($P^o_{IPA}$ = 0.022 atm; $W/F^o_{IPA}$ = 0.043 g s/μmol).

contrary, the thermal treatments performed to carbon C1-450 after the activation process results in a decrease in the carbon activity, being this decrease more pronounced at higher thermal treatment temperatures. The thermal treatment reduces the amount of surface oxygen and the surface acidity, and so, decreases the activity of the carbons for 2-propanol decomposition. The sample obtained by carbonization at 450 °C without phosphoric acid, C-450, shows a 2-propanol conversion lower than 10% at 350 °C (not represented), much lower than those observed for the carbons activated with phosphoric acid, as a consequence of a much lower surface acidity. The lower activity of this char may also be associated to its lower surface area (256 m²/g). However, we have previously reported [7] that a commercial activated carbon with a similar surface area, but significantly lower surface acidity needs much higher temperatures for reaching similar 2-propanol conversion than carbons activated with phosphoric acid. Furthermore, activated carbons prepared by chemical activation with phosphoric acid at different conditions that presented higher surface areas, but retained lower amount of surface phosphorus (lower acidity), showed lower activity for alcohol dehydration than those containing higher amount of surface phosphorus groups. This fact and the fact that carbonization of biomass does not produce carbons with relevant acidity suggest that the lower activity of C-450 char is mainly due to its lower surface acidity, beside its lower surface area.

The 2-propanol decomposition yields only dehydration products, propylene and di-isopropyl ether, for all the catalysts studied. Fig. 8 represents the evolution of the conversion and selectivity to
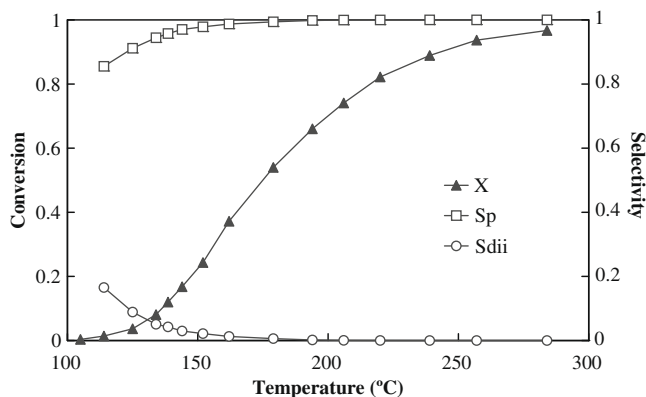
propylene (Sp) and to di-isopropyl ether (Sdii) with the reaction temperature for carbon C1-450 at an inlet 2-propanol partial pressure of 0.022 atm and a space time of 0.043 g s/μmol. The main reaction product is propylene with lower amounts of di-isopropyl ether. Only at low temperatures and low conversion values the selectivity to the ether is significant. An increase in the reaction temperature results in higher olefin selectivity. At temperatures higher than 175 °C, the 2-propanol dehydration on C1-450 is 100% selective to propylene. The other carbon catalysts show a similar behavior.

Fig. 9 represents the 2-propanol conversion and selectivities to propylene and di-isopropyl ether with the reaction time at 170 °C for C1-450 carbon. The 2-propanol conversion does not decrease with the reaction time, but increases slightly from around 0.5 up to 0.6. The selectivities to both propylene and di-isopropyl ether does not change with the reaction time, suggesting that the catalyst obtained does not suffer deactivation during the reaction, at the conditions analyzed in this work.

Fig. 10 shows the effect of the inlet water vapor partial pressure in the conversion values for the C1-450 carbon at 155 °C. The variation of the water vapor partial pressure showed little effect on the 2-propanol conversion and on the product distribution, which probably indicates a negligible adsorption of water vapor on the active sites during 2-propanol dehydration reaction. In this sense, adsorption of water vapor was not considered in the development of the kinetic model.

Fig. 11 represents 2-propanol conversions at different partial pressures of 2-propanol and constant space time ($W/F^o_{IPA}$ = 0.043 g s/μmol), at reaction temperatures of 125, 140,
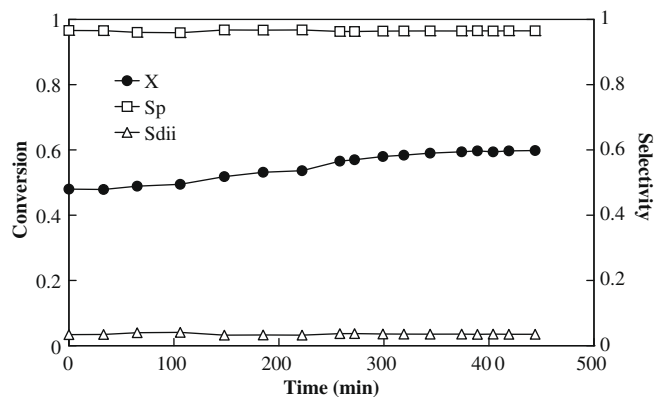


**Fig. 9.** Evolution of the 2-propanol conversion and selectivity to propylene (Sp) and di-isopropyl ether (Sdii) with the reaction time at 170 °C on the C1-450 catalysts ($P^o_{IPA}$ = 0.022 atm; $W/F^o_{IPA}$ = 0.043 g s/μmol).



**Fig. 8.** Conversion of 2-propanol and selectivity to propylene (Sp) and to di-isopropyl ether (Sdii) as a function temperature for the C1-450 catalyst ($P^o_{IPA}$ = 0.022 atm; $W/F^o_{IPA}$ = 0.043 g s/μmol).
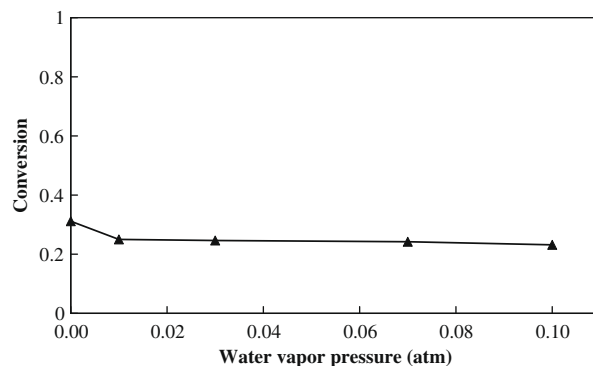


**Fig. 10.** Evolution of the 2-propanol conversion with the inlet water vapor partial pressure for the C1-450 catalysts at 155 °C ($P^o_{IPA}$ = 0.022 atm; $W/F^o_{IPA}$ = 0.043 g s/μmol).
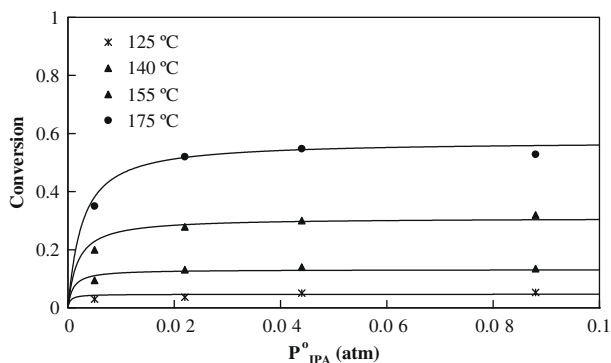
**Fig. 11.** Evolution of 2-propanol conversion with inlet partial pressure of 2-propanol at different temperatures and constant space time ($W/F^o_{IPA}$ = 0.043 g s/µmol).
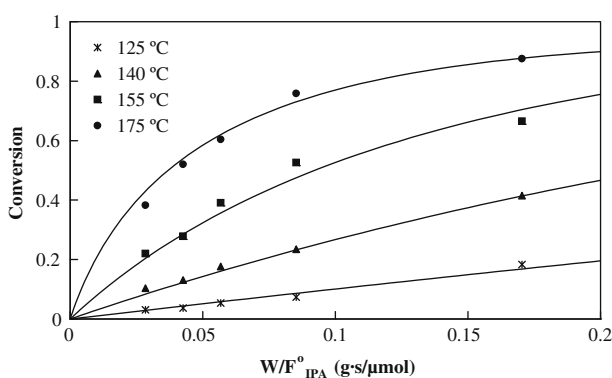


**Fig. 12.** Evolution of 2-propanol conversion with space time at different temperatures and constant 2-propanol inlet partial pressure ($P^o_{IPA}$ = 0.022 atm).

155 and 170 °C for the C1-450 carbon. At $P^o_{IPA} < 0.02$, the conversion increases with the 2-propanol partial pressure. This increase is higher at high temperatures. At partial pressures of 2-propanol higher than 0.02 atm, the conversion remains almost constant. Fig. 12 depicts the evolution of the conversion of 2-propanol with the space time (up to values of around 0.170 g s/µmol) at a 2-propanol partial pressure of 0.022 atm and temperatures between 125 and 170 °C. Alcohol conversion increases with the space time at all the temperatures studied.

Integral reactor behavior was used for the interpretation of the experimental data. To this purpose, the reactor continuity, Eq. (2), was integrated numerically to calculate the exit conversion of 2-propanol dehydration reaction.

$$\frac{dX_{IPA}}{d\left(\frac{W}{F^o_{IPA}}\right)} = r_{IPA} \tag{2}$$

In Eq. (2), $r_{IPA}$ represents the conversion rate of 2-propanol, $X_{IPA}$ is the total conversion of 2-propanol and $(W/F^o_{IPA})$ is the 2-propanol space time. The following suppositions were assumed: homogeneous distribution of active sites on the catalyst surface, catalyst is assumed to operate at steady-state conditions, diffusional constraints and transport limitations are negligible (as proven theoretically) and changes in temperature and pressure within the reactor were neglected. As the total conversion to di-isopropyl ether is always lower than 1%, the intermolecular dehydration to the ether was not considered in the kinetic model resolution.

Two Langmuir–Hinshellwood mechanisms were considered, assuming that the surface reaction was an E1 (two-step) or an E2 (one-step) elimination mechanism.

### 3.2.1. E1 model

E1 mechanism involves the initial protonation of the OH group in the molecule of 2-propanol, followed by the cleavage of the CO bond producing a carbocation (CARB) and a water molecule as leaving group. This step is unimolecular and limits the rate of the reaction. The second step is a fast deprotonation of the carbocation by the loss of one β hydrogen and the formation of the double bond, C=C, and thus the propylene molecule (PROPY). The elementary steps for the proposed model are shown in the following equations, in which ∗ represents an acid active site:
2-Propanol adsorption:

$$IPA(g) + * \overset{K_{IPA}}{\leftrightarrow} IPA^* \tag{3}$$

Surface reaction:

$$IPA^* \overset{k_{CARB}}{\to} CARB^* + H_2O(g) \tag{4}$$

$$CARB^* \overset{k_{PROPY}}{\to} PROPY^* \tag{5}$$

Propylene desorption:

$$PROPY^* \overset{1/K_{PROPY}}{\leftrightarrow} + * \tag{6}$$

The adsorption of 2-propanol is assumed to take place molecularly and in quasi-equilibrium between the adsorbed and vapor-phase 2-propanol. The formation of the propylene molecule is supposed to occur in two sequential elementary steps. In the first step, the formation of the adsorbed carbocation and the gas-phase water molecule is assumed to be the rate-determining step (rds), whereas in the second step, the formation of adsorbed propylene molecule takes place. In the last step, a fast desorption of propylene molecules occurs. With these considerations, the global reaction rate is

$$-r_{IPA} = r_{CARB} = k_{CARB} \cdot \theta_{IPA} \tag{7}$$

where $k_{CARB}$ is the forward rate constant of the reaction (4) and $\theta_{IPA}$ is the fractional coverage of 2-propanol. From the consideration of quasi-equilibrium for adsorption of 2-propanol and desorption of propylene it can be obtained

$$\theta_{IPA} = K_{IPA} \cdot P_{IPA} \cdot \theta_V \tag{8}$$

$$\theta_{PROPY} = K_{PROPY} \cdot P_{PROPY} \cdot \theta_V \tag{9}$$

where $\theta_V$ and $\theta_{PROPY}$ are the fraction of vacant acid sites and propylene occupied sites, respectively, $K_{IPA}$ and $K_{PROPY}$ are the adsorption constants and $P_{IPA}$ and $P_{PROPY}$ are the partial pressures of 2-propanol and propylene, respectively. Assuming a pseudo-steady state for the adsorbed carbocation formation, the next expression is obtained:

$$\frac{d\theta_{CARB}}{dt} = k_{CARB} \cdot \theta_{IPA} - k_{PROPY} \cdot \theta_{CARB} \approx 0 \Rightarrow \theta_{CARB} = \frac{k_{CARB} \cdot \theta_{IPA}}{k_{PROPY}} \tag{10}$$

The site balance is shown in the following equation,

$$1 = \theta_V + \theta_{IPA} + \theta_{CARB} + \theta_{PROPY} \tag{11}$$

and rearranging the Eqs. (8)–(11) yields,

$$\theta_V = \frac{1}{1 + K_{IPA} \cdot P_{IPA} + \frac{k_{CARB} \cdot K_{IPA} \cdot P_{IPA}}{k_{PROPY}} + K_{PROPY} \cdot P_{PROPY}} \tag{12}$$

and the final rate expression results in

$$-r_{IPA} = r_{CARB} = \frac{k_{CARB} \cdot K_{IPA} \cdot P_{IPA}}{1 + K_{IPA} \cdot P_{IPA} + \frac{k_{CARB} \cdot K_{IPA} \cdot P_{IPA}}{k_{PROPY}} + K_{PROPY} \cdot P_{PROPY}} \tag{13}$$

### 3.2.2. E2 model

This model assumes a Langmuir–Hinshelwood mechanism in which the surface reaction is an E2 elimination in a single step. In this case, both the leaving group, OH and the β proton depart

simultaneously in a single concerted step. The elementary steps for this mechanism are shown below.

2-Propanol adsorption:

$$IPA(g) + * \overset{K_{IPA}}{\leftrightarrow} IPA^* \tag{14}$$

Surface reaction:

$$IPA^* \overset{k_{PROPY}}{\rightarrow} PROPY^* + H_2O(g) \tag{15}$$

Propylene desorption:

$$PROPY^* \overset{1/K_{PROPY}}{\leftrightarrow} PROPY(g) + * \tag{16}$$

In this model, as for E1 model, the 2-propanol adsorption is assumed to take place molecularly and in quasi-equilibrium between the adsorbed and vapor-phase 2-propanol. The formation of the propylene molecule is supposed to occur in a single concerted step. Again, desorption of the molecules of propylene is assumed to be faster than propylene adsorbed formation. Considering the formation of adsorbed propylene molecule like the rate-determining step, the global reaction rate can be written as

$$-r_{IPA} = r_{PROPY} = k_{PROPY} \cdot \theta_{IPA} \tag{17}$$

where $k_{PROPY}$ is the forward rate constant of the reaction (15) and $\theta_{IPA}$ is the fractional coverage of 2-propanol. The expressions for adsorption of 2-propanol and desorption of propylene are Eqs. (8) and (9), respectively. In this model, only molecules of 2-propanol and propylene could adsorb on the active sites of the carbon surface, and so, the site balance is

$$1 = \theta_V + \theta_{IPA} + \theta_{PROPY} \tag{18}$$

with the Eqs. (8) and (9) leads to

$$\theta_V = \frac{1}{1 + K_{IPA} \cdot P_{IPA} + K_{PROPY} \cdot P_{PROPY}} \tag{19}$$

and the final rate expression results in

$$-r_{IPA} = r_{PROPY} = \frac{k_{PROPY} \cdot K_{IPA} \cdot P_{IPA}}{1 + K_{IPA} \cdot P_{IPA} + K_{PROPY} \cdot P_{PROPY}} \tag{20}$$

For both models, the kinetic parameters were estimated by a Runge–Kutta method combined with an optimization routine based in the Levenberg–Marquardt [50,51] algorithm, minimizing the error function:

$$error = \sum_i \left( X_{exp,i} - X_{sim,i} \right)^2 \tag{21}$$

where $X_{exp}$ is the value of the steady-state conversion obtained experimentally and $X_{sim}$ is the simulated value. The dependence of the kinetic parameters with the temperature was considered to follow an Arrhenius law for the kinetic constant (Eqs. (23) and (24)) or a Van't Hoff law for the adsorption constants (Eqs. (22) and (25)).

$$K_{IPA} = K_{oIPA} \cdot \exp \left( \frac{-\Delta H_{IPA}}{R \cdot T} \right) \tag{22}$$

$$k_{CARB} = k_{oCARB} \cdot \exp \left( \frac{-Ea_{CARB}}{R \cdot T} \right) \tag{23}$$

$$k_{PROPY} = k_{oPROPY} \cdot \exp \left( \frac{-Ea_{PROPY}}{R \cdot T} \right) \tag{24}$$

$$K_{PROPY} = K_{oPROPY} \cdot \exp \left( \frac{-\Delta H_{PROPY}}{R \cdot T} \right) \tag{25}$$

where $k_{oi}$, $K_{oi}$ are the preexponential factors, $\Delta H_{IPA}$ and $\Delta H_{PROPY}$ are the enthalpies of adsorption of 2-propanol and propylene, respectively, and $Ea_{CARB}$ and $Ea_{PROPY}$ are the activation energies for the reactions represented in Eqs. (4) and (5) and (15), respectively.

Both models fit properly the experimental data with low error values, although slightly lower values were obtained for E1 model (error = 0.031) than for E2 model (error = 0.037). This could be due to that both mechanisms are similar and, probably, both mechanisms occur simultaneously over the carbon surface. The result of the model E1 application to the experimental data is shown in Figs. 11 and 12 as solid lines (symbols are the experimental values). Fig. 13 represents the simulated conversion, $X_{sim}$, assuming the E1 model, versus the conversion obtained experimentally, $X_{exp}$ for dehydration of 2-propanol on C1-450 catalysts. The result shows that E1 model represents properly the experimental data.

The values of the parameters obtained by numerical simulation to both models, E1 and E2, are summarized in Table 2. The activation energy for the rate-determining step of both models is very similar, nearly 98 kJ/mol. This fact indicates that formation of the carbocation through and E1 mechanism and the formation of the propylene by an E2 mechanism occur at a very similar rate, and, therefore, it is probably that both mechanisms take place simultaneously. The literature shows a broad spectrum of apparent activation energy values for this reaction, ranging from 12 to 133 kJ/mol [6, 52-54]. This large variation in the activation energy values could be due to the different type of interaction between 2-propanol molecules and the catalyst surfaces. Also, diffusional limitations may reduce the value of the apparent activation energy.

In order to corroborate the validity of the proposed reaction models, some requirements have to be fulfilled [55]. The enthalpies of adsorption must be negative, as adsorption is always exothermic. This condition is satisfied for both models, since $\Delta H_{IPA}$ and $\Delta H_{PROPY}$ are negative. The standard entropy of adsorption, $\Delta S_{ad}^0$, must fulfill two additional requirements: (i) $\Delta S_{ad}^0$ must be negative and (ii) $\Delta S_{ad}^0$ must have an absolute value smaller than $S_g^0$, the standard entropy in gas phase [56,57]. The values of $S_g^0$ for 2-propanol and propylene are 181.1 and 266.8 J/mol K, respectively [58]. The standard enthalpy and entropy in gas phase are related by the expression:

$$Ln(K) = \frac{-\Delta H_{ad}^0}{R \cdot T} + \frac{\Delta S_{ad}^0}{R} \tag{26}$$

The values of the standard entropy of adsorption could be obtained taking into account that at $1/T = 0$, $Ln(K_{oi}) = \Delta S/R$. The values of $\Delta S_{ad}^0$ for 2-propanol and propylene for model E1 are $-135.5$ and $-38.3$ J/mol K, respectively, and these values for model E2 are $-128.8$ and $-29.5$ J/mol K, respectively. Both models yield standard adsorption entropies that fulfill the aforementioned requirements.

Fig. 14 represents the FTIR spectrum obtained at room temperature of C1-450 activated carbon after reaction for 2 h at 150 °C with 2-propanol ($P_{IPA}^o = 0.022$ atm, $W/F_{IPA}^o = 0.043$ g s/μmol). The spectrum of the carbon that was not subject to reaction has been
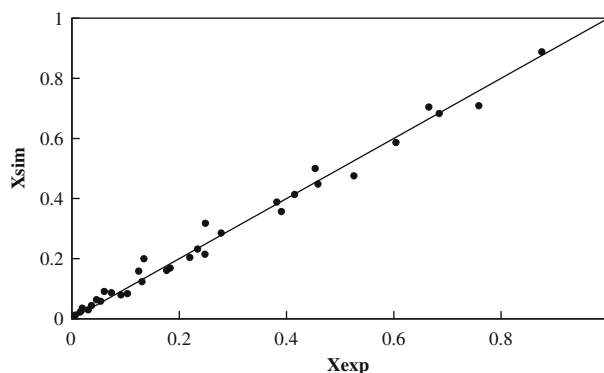


Fig. 13. Conversion simulated by E1 model versus conversion obtained experimentally.

**Table 2**
Optimized kinetic parameters for mechanisms E1 and E2.

| Model | $K_{IPA}$ | | $k_{CARB}$ | | $k_{PROPY}$ | | $K_{PROPY}$ | |
|-------|-----------|----------------------------|------------|-----------------------|-------------|-----------------------|-------------|--------------------------|
|       | $K_{oIPA}$ (atm$^{-1}$) | $\Delta H_{IPA}$ (kJ/mol) | $k_{oCARB}$ (mol/g s) | Ea$_{CARB}$ (kJ/mol) | $k_{oPROPY}$ (mol/g s) | Ea$_{PROPY}$ (kJ/mol) | $K_{oPROPY}$ (atm$^{-1}$) | $\Delta H_{PROPY}$ (kJ/mol) |
| E1 | $8.3 \times 10^{-8}$ | −78.3 | $8.7 \times 10^{+6}$ | 98.5 | $1.0 \times 10^{+7}$ | 65.0 | $1.0 \times 10^{-2}$ | −35.8 |
| E2 | $1.8 \times 10^{-7}$ | −75.6 | – | – | $8.9 \times 10^{+6}$ | 98.3 | $2.9 \times 10^{-2}$ | −33.4 |
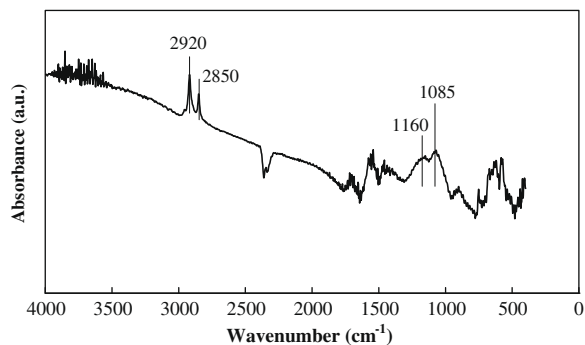


**Fig. 14.** FTIR spectrum of C1-450 carbon catalyst after 2-propanol adsorption.

subtracted. It should be noted that it can be difficult to discern between surface isopropoxide species and molecularly adsorbed isopropanol without other additional characterization techniques. The reaction of 2-propanol with the carbon surface produces an increase in the two bands clearly observed at 2920 and 2850 cm$^{-1}$ probably as a consequence of the C—H stretching vibrations of undissociated 2-propanol molecules. The absence of a defined band at around 3663 cm$^{-1}$ suggested a weak interaction between the adsorbed 2-propanol and the carbon surface [55]. The peaks at 1160 and 1085 cm$^{-1}$ are assigned to the vibration of P=O groups and of P—O$^-$, respectively. Both peaks may be increased by the adsorption of cationic species (isopropoxide or carbocation) on the carbon surface. The FTIR spectrum of the carbon C1-450 after

reaction with 2-propanol suggests the coexistence of at least two adsorbed species, one undissociated as 2-propanol molecules and the other one dissociated forming isopropoxide or carbocation species [59–61]. These results, although not conclusive, may support that both mechanisms take place simultaneously during dehydration reaction, an E1 mechanism in which the reaction goes through intermediate isopropoxide–carbocation species and the E2 mechanism in which the propylene is formed from 2-propanol adsorbed molecules.

Fig. 15 outlines the surface reaction mechanisms proposed, E1 and E2. The 2-propanol molecule is adsorbed on the OH group of the phosphate, probably by hydrogen bonding. The adsorbed 2-propanol could coexist with the protonated species, as shown by FTIR analysis, formed by the transfer of a proton from the Brönsted acid site that yields isopropoxide–carbocation ions in equilibrium, which could be considered as only one species in the reaction mechanism. Both species produce the olefin by surface elimination mechanisms. Via E1 mechanism, the adsorbed carbocation is formed, and subsequently a β hydrogen departs and the propylene is obtained. Via E2, the adsorbed olefin is produced in a single concerted step, with the loss of the water molecule and the deprotonation in β happen simultaneously.

## 4. Conclusions

The chemical activation of hemp residues with $H_3PO_4$ results in carbons with a high surface acidity because of the residual phos-
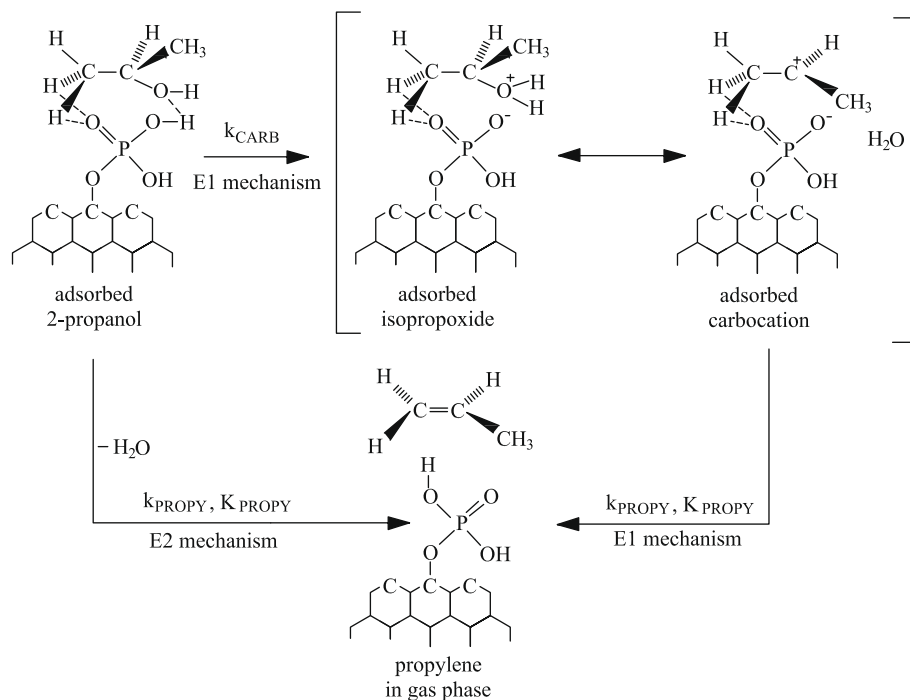


**Fig. 15.** Scheme of the proposed surface reaction mechanisms from a 2-propanol molecule adsorbed on a phosphate group.

phorus groups with a high thermal stability that remain in the carbon surface.

The TPD–CO profiles are mainly characterized by a considerable amount of CO desorbed at high temperatures ($T > 700$ °C) associated to the decomposition of the $C-O-PO_3$ and $C-PO_3$ groups formed during the activation process. The surface acidity of the carbons, determined by $NH_3$–TPD, seems to be related to the phosphorus retained on the carbon surface. Irreversible adsorption of organic bases, such as pyridine and 2,6-dimethyl pyridine, suggests the presence of Brönsted acid sites.

Conversion of 2-propanol yields only dehydration products and is highly selective to propylene, with very low amounts of di-isopropyl ether observed only at low conversion values. Kinetic interpretation of the experimental data was performed using two elimination mechanisms; an E1 mechanism (two-step mechanism) and an E2 mechanism (one-step mechanism). The rate expressions derived from both models represent properly the experimental results, suggesting that probably the two mechanisms occur simultaneously. This supposition is supported by the similar rate constant obtained for the rate-determining step of both models, formation of the carbocation in E1 mechanism and formation of the propylene in the E2 mechanism. The activation energy of the rds of both models is very similar, nearly 98 kJ/mol. This fact indicates that formation of the carbocation through and E1 mechanism and formation of the propylene by an E2 mechanism occur at a very similar rate, and, therefore, it is probably that both mechanisms take place simultaneously. Furthermore, the FTIR spectrum of the carbon C1-450 after reaction with 2-propanol suggests the coexistence of at least two adsorbed species, one undissociated as 2-propanol molecules and the other one dissociated forming isopropoxide–carbocation species.

## Acknowledgments

## References

[1] C. Branca, P. Giudicianni, C . Di Blasi, Ind. Eng. Chem. Res. 43 (2003) 3190.
[2] A.E. Pütün, A. Özcan, H.F. Gerçel, E. Pütün, Fuel 8 (2001) 1371.
[3] J.D. Adjaye, S.P.R. Katikaneni, N.N. Bakhshi, Fuel Process. Technol. 48 (1996) 115.
[4] A.G. Gayubo, A.T. Aguayo, A. Atutxa, R. Aguado, J. Bilbao, Ind. Eng. Chem. Res. 43 (2004) 2610.
[5] A.G. Gayubo, A.T. Aguayo, A. Atutxa, R. Aguado, M. Olazar, J. Bilbao, Ind. Eng. Chem. Res. 43 (2004) 2619.
[6] J.M. Campelo, A. Garcia, J.F. Herencia, D. Luna, J.M. Marinas, A.A. Romero, J. Catal. 151 (1995) 307.
[7] J. Bedia, J. Márquez, J. Rodríguez-Mirasol, T. Cordero, Carbon 47 (2009) 286.
[8] H. Koempel, W. Liebner, Stud. Surf. Sci. Catal. 167 (2007) 261–267.
[9] L.R. Radovic, F. Rodríguez-Reinoso, in: P.A. Thrower (Ed.), Chemistry and Physics of Carbon, vol. 25, Marcel Dekker, New York, 1997, pp. 243–358.
[10] R.W. Coughlin, Ind. Eng. Chem. Prod. Res. Develop. 8 (1964) 23.
[11] F. Rodríguez-Reinoso, M. Molina-Sabio, Carbon 30 (1992) 1111.
[12] O. Ioannidou, A. Zabaniotou, Renew Sustain Energy Rev 11 (2007) 1966.
[13] J. Rodríguez-Mirasol, J. Bedia, T. Cordero, J.J. Rodríguez, Sep. Sci. Technol. 40 (2005) 3113.
[14] J.M. Rosas, J. Bedia, J. Rodríguez-Mirasol, T. Cordero, Fuel 88 (2009) 19.
[15] C.A. Leon y Leon, L.R. Radovic, in: P.A. Thrower (Ed.), Chemistry and Physics of Carbon, M. Dekker, New York, 1992, pp. 213–310.
[16] G.S. Szymański, G. Rychlicki, Carbon 31 (1993) 247.
[17] C. Moreno-Castilla, F. Carrasco-Marín, C. Parejo-Pérez, M.V. López Ramón, Carbon 39 (2001) 869.
[18] J.L. Figueiredo, M.F.R. Pereira, M.M.A. Freitas, J.J.M. Órfao, Carbon 37 (1999) 1379.
[19] J.M. Rosas, J. Bedia, J. Rodríguez-Mirasol, T. Cordero, Ind. Eng. Chem. Res. 47 (2008) 1288.
[20] E. González-Serrano, T. Cordero, J. Rodríguez-Mirasol, L. Cotoruelo, J.J. Rodríguez, Water Res. 38 (2004) 3043.
[21] X. Wu, L.R. Radovic, Carbon 44 (2006) 151.
[22] P.J. Hall, J.M. Calo, Energy Fuels 3 (1989) 370.
[23] A.M. Puziy, O.I. Poddubnaya, A. Martínez-Alonso, F. Suárez-García, J.M.D. Tascón, Carbon 43 (2005) 2857.
[24] J. Coates, in: R.A. Meyers (Ed.), Interpretation of Infrared Spectra, A Practical Approach, John Wiley & Sons Ltd., Chichester, 2000, pp. 10815–10837.
[25] J. Zawadzki, in: P.A. Thrower (Ed.), Infrared Spectroscopy in Surface Chemistry of Carbons, Marcel Dekker, New York, 1989, pp. 147–386.
[26] P. Vinke, M. van der Eijk, M. Verbree, A.F. Voskamp, H. van Bekkum, Carbon 32 (1994) 675.
[27] M.S. Solum, R.J. Pugmire, M. Jagtoyen, F. Derbyshire, Carbon 33 (1995) 1247.
[28] Spectroscopic Tools. <http://www.chem.unipotsdam.de/tools/index.html>.
[29] L.J. Bellamy, The Infra-red Spectra of Complex Molecules, Wiley, New York, 1954.
[30] D.E.C. Corbridge, J. Appl. Chem. 6 (1956) 456.
[31] G. Socrates, Infrared Characteristic Group Frequencies, Wiley, New York, 1994.
[32] R. Xie, B. Qu, K. Hu, Polym. Degrad. Stab. 72 (2001) 313.
[33] S. Bourbigot, M. Le Bras, R. Delobel, Carbon 33 (1995) 283.
[34] F.M. Bautista, J.M. Campelo, A. Garcia, D. Luna, J.M. Marinas, A.A. Romero, M.R. Urbano, J. Catal. 172 (1997) 103.
[35] H.A. Benesi, J. Catal. 28 (1973) 176.
[36] H. Knözinger, H. Krietenbrink, P. Ratnasamy, J. Catal. 48 (1977) 436.
[37] A. Corma, C. Rodellas, V. Fornes, J. Catal. 88 (1984) 374.
[38] M.H. Healy, L.F. Wieserman, E.A. Arnett, K. Wefers, Langmuir 5 (1989) 114.
[39] A. Travert, O.V. Manoilova, A.A. Tsyganenko, F. Maugé, J.C. Lavalley, J. Phys. Chem. B 106 (2002) 1350.
[40] G. Turnes Palomino, J.J. Cuart Pascual, M. Rodríguez Delgado, J. Bernardo Parra, C. Otero Areán, Mater. Chem. Phys. 85 (2004) 145.
[41] P.A. Jacobs, C.F. Heylen, J. Catal. 34 (1974) 267.
[42] C. Petit, F. Maugé, J.C. Lavalley, Stud. Surf. Sci. Catal. 106 (1997) 157.
[43] A.A. Tsyganenko, E.N. Storozheva, O.V. Manoilova, T. Lesage, M. Daturi, J.C. Lavalley, Catal. Lett. 70 (2000) 159.
[44] C. Morterra, G. Cerrato, G. Meligrana, Langmuir 17 (2001) 7053.
[45] J.F. Moulder, W.F. Stickle, P.E. Sobol, K.D. Bomben, in: J. Chastain, R.C. King Jr. (Eds.), Handbook of X-ray Photoelectron Spectroscopy, Physical Electronics Inc., Eden Prairie, MN, 1995, pp. 4872–4875.
[46] D.E. Meras, Chem. Eng. Sci. 26 (1971) 1361.
[47] C.N. Satterfield, Heterogeneous Catalysis in Practice, McGraw-Hill, New York, 1991.
[48] J.A. Moulijn, A. Tarfaoui, F. Kapteijn, Catal. Today 11 (1991) 1.
[49] H. Gierman, Appl. Catal. 43 (1988) 277.
[50] K. Levenberg, Q. Appl. Math. 2 (1944) 164.
[51] D. Marquardt, SIAM J. Appl. Math. 11 (1963) 431.
[52] M.A. Aramendia, V. Borau, C. Jiménez, J.M. Marinas, A. Porras, F.J. Urbano, J. Catal. 161 (1996) 829.
[53] W. Turek, J. Haber, A. Krowiak, Appl. Surf. Sci. 252 (2005) 823.
[54] P. Trens, V. Stathopoulos, M.J. Hudson, P. Pomonis, Appl. Catal. A 263 (2004) 103.
[55] R.M. Rioux, M.A. Vannice, J. Catal. 216 (2003) 362.
[56] M. Boudart, D.E. Meras, M.A. Vannice, Ind. Chem. Belge 32 (1967) 281.
[57] M.A. Vannice, S.H. Hyun, B. Kalpalci, W.C. Liauh, J. Catal. 56 (1979) 358.
[58] J.A. Deon, Lange's Handbook of Chemistry, 15th ed., McGraw-Hill, New York, 1999. p. 6.42.
[59] J. Zawadzki, M. Wisniewski, J. Weber, O. Heintz, B. Azambre, Carbon 39 (2001) 187.
[60] J.L. Davis, M.A. Barteau, Surf. Sci. 235 (1990) 235.
[61] R.F. Rossi, G. Busca, V. Lorenzelli, O. Saur, J.C. Lavalley, Langmuir 3 (1987) 52.